ELSEVIER

Chemosphere

Aqueous Picloram Degradation by Hydroxyl Radicals: Unveiling Mechanism, Kinetics, and Ecotoxicity through Experimental and Theoretical Approaches

Flávio O. Sanches-Neto[1]*, Bruno Ramos[2], Arlen M. Lastre-Acosta[2], Antonio Carlos S. C. Teixeira[2], Valter H. Carvalho-Silva[1,3]*

[1]Instituto de Química, Universidade de Brasília, Caixa Postal 4478, 70904-970, Brasília, Brazil;

[2]Research Group in Advanced Oxidation Processes (AdOx), Department of Chemical Engineering, Escola Politécnica, University of São Paulo, São Paulo 05508-010, Brazil;

[3]Modeling of Physical and Chemical Transformations Division, Theoretical and Structural Chemistry Group, Research and Postgraduate Center, Goiás State University, 75132-903, Anápolis, Brazil.

*Correspondence: flavio_olimpio@outlook.com (ORCID: 0000-0002-0664-171X); fatioleg@gmail.com (ORCID: 0000-0002-7411-0099)

ABSTRACT. Pesticides are chemical compounds widely used to combat pests in crops, and they thus play a key role in agricultural production. However, due to their persistence in aquatic environments, even at low concentrations, their use has been considered an environmental problem and caused concern regarding the adverse effects on human health. This paper reports, for the first time, the mechanisms, kinetics, and an evaluation of the toxicity of picloram degradation initiated by •OH radicals in the aqueous environment using quantum chemistry and computational toxicology calculations. The rate constants are calculated using a combination of formulations derived from the

Transition State Theory in a realistic temperature range (250-310 K). The results indicate that the two favorable pathways (R1 and R5) of •OH-based reactions occur by addition to the pyridine ring. The calculated rate constant at 298 K is compared with the overall second-order reaction rate constant, quantified herein experimentally via the competition kinetics method and data available in the literature showing an excellent agreement. The toxicity assessment and a photolysis study provide important information: i) picloram and the majority of degradation products are estimated as harmful; however, ii) these compounds can suffer photolysis in sunlight. The results of the present study can help understand the mechanism of picloram, also providing important clues regarding risk assessment in aquatic environments as well as novel experimental information.

Keywords: Organic contaminant degradation, Pesticides, d-TST, AOPs, DFT

1. Introduction

It is well known that the use of pesticides plays a key role in agricultural production (Lin et al., 2018; Tomlin and others, 2009) and in global public health (Organization and others, 1990; Planas et al., 1997), and contributes as an important factor for global economic stability (Seufert et al., 2012; Vasileiadis, 2017). However, in recent years, the widespread use of pesticides has caused significant consequences for the environment and raised concerns due to their carcinogenic and toxic effects on non-target organisms (Canna-Michaelidou and Nicolaou, 1996; Tremolada et al., 2004). Pesticides are complex chemical compounds used to combat pests, such as insects and fungi (Ikehata and El-Din, 2006; Organization and others, 2006). Detailed knowledge of the physical-chemical properties of these species is

essential for understanding the impact they might have in the environment (Socorro et al., 2016). The volatility of these compounds, for instance, can contribute to air contamination by evaporation during application (Aktar et al., 2009; Waite et al., 1999); their solubility in water determines the degree to which they can contaminate groundwater (Ghauch, 2001; Luo et al., 2014), and contribute to soil desertification by leaching (Graça et al., 2019) and erosion (Bereswill et al., 2012; Khan, 2016). Many efforts have been devoted to removing pesticides from surface waters, groundwater and industrial effluents because of the adverse effects these species might have on living organisms (An et al., 2014; Cardoso and Valim, 2006). Various technologies, such as dry and wet deposition (Ghauch, 2001; Sauret et al., 2009), adsorption filters (Cardoso and Valim, 2006; Suo et al., 2019), biological treatments (Lafi and Al-Qodah, 2006; Zapata et al., 2010), and Advanced Oxidation Processes (AOPs) (An et al., 2014; Oturan and Aaron, 2014) have been developed in a collective effort to remove and/or destroy dangerous contaminants before their disposal in the environment.

Pyridine and derivative compounds have attracted extensive attention due to their occurrence in the environment and the hazardous effects they have on ecosystems and on human health (Abramović et al., 2011; Stapleton et al., 2010). One of the most common pyridine-derived pesticides is picloram (4-amino-3,5,6-trichloro-2-pyridinocarboxylic), a herbicide used for controlling weeds in wheat, barley, oats, and woody plant species (Cardoso and Valim, 2006; Ghauch, 2001; Haag and David Yao, 1992; Hedlund and Youngson, 1972). The

toxicity of picloram is considered moderate to high (Abramović et al., 2011; Wauchope et al., 1992), with half-lives in the range 20-300 days (Rahman and Muneer, 2005; Socorro et al., 2016). Furthermore, its photodegradation on the soil surface with the use of aerobic microorganisms is mediated by its efficient solubility in water (Abramović et al., 2011; Ghauch, 2001). All these properties combined with its persistence in the soil confirm the risk of groundwater contamination. In fact, picloram has already been detected in ten American states by the United States Environmental Protection Agency (Ghauch, 2001; Howard, 2017). These features have been supported by several studies of picloram degradation in aqueous solution. Ghauch (Ghauch, 2001) studied the degradation of picloram using zero-valent iron powder in an aerobic conical apparatus, in which the pollutant was converted into 4-amino-2-pyridylcarbinol, a substance considered environmentally dangerous. Cardoso and Valim (Cardoso and Valim, 2006) investigated the ability of layered double hydroxides to adsorb picloram from aqueous solutions, achieving 96% adsorption after 6 hours; however, this physical treatment alone does not promote contaminant degradation. Özcan et al. (Özcan et al., 2008) used the electro-Fenton process to remove picloram from aqueous solution using current density and catalyst concentration of 300 mA and 0.2 mM Fe^{3+}, respectively. The authors reported a reaction rate constant of 4.53×10^{-12} $cm^3 \cdot molecule^{-1} \cdot s^{-1}$ at 298.15 K. The reaction rate constant of the degradation of picloram with $^{\bullet}OH$ radicals has only been reported at ambient temperatures. Other authors have carried out kinetic and mechanistic studies of picloram photodegradation with titanium dioxide, identifying

several intermediates and reaction pathways (Abramović et al., 2011). Recently, Coledam et al. (2018) used four methods based on the production of •OH radicals to evaluate the oxidation and mineralization of picloram: these results support the photo-Fenton HOCl/UVC process as an efficient option to treat aqueous organic contaminants.

The reaction of •OH radicals with organic pollutants is often complex and involves three possible mechanisms (An et al., 2014; Manonmani et al., 2020, 2019; Mei et al., 2019): i) addition of •OH to an aromatic ring or other unsaturated bonds, ii) hydrogen-atom abstraction, and/or iii) single electron transfer. From an experimental perspective, the identification and elucidation of the mechanisms shown above are analytically challenging, complex, expensive and equipment-dependent (An et al., 2014; Mei et al., 2019; Milenković et al., 2020). The laborious experimental procedures involved in distinguishing and quantifying the reaction mechanisms of •OH radicals with organic molecules make quantum theoretical calculations appear as an advantageous protocol to obtain a more detailed picture of the mechanisms and kinetics of such reaction systems. Nevertheless, to the best of our knowledge, there are no theoretical studies regarding the attack of •OH radicals on picloram molecules. Thus, the focus of this work is to provide a detailed understanding of the mechanism and kinetics of picloram degradation mediated by •OH radicals using a blend of quantum chemistry calculations, reaction rate theory, and experimental kinetics procedures. In addition, we provide an evaluation of the

photolysis and toxicity of picloram and its degradation products using a TD-DFT procedure and an Ecological Structure-Activity Relationships predictive model.

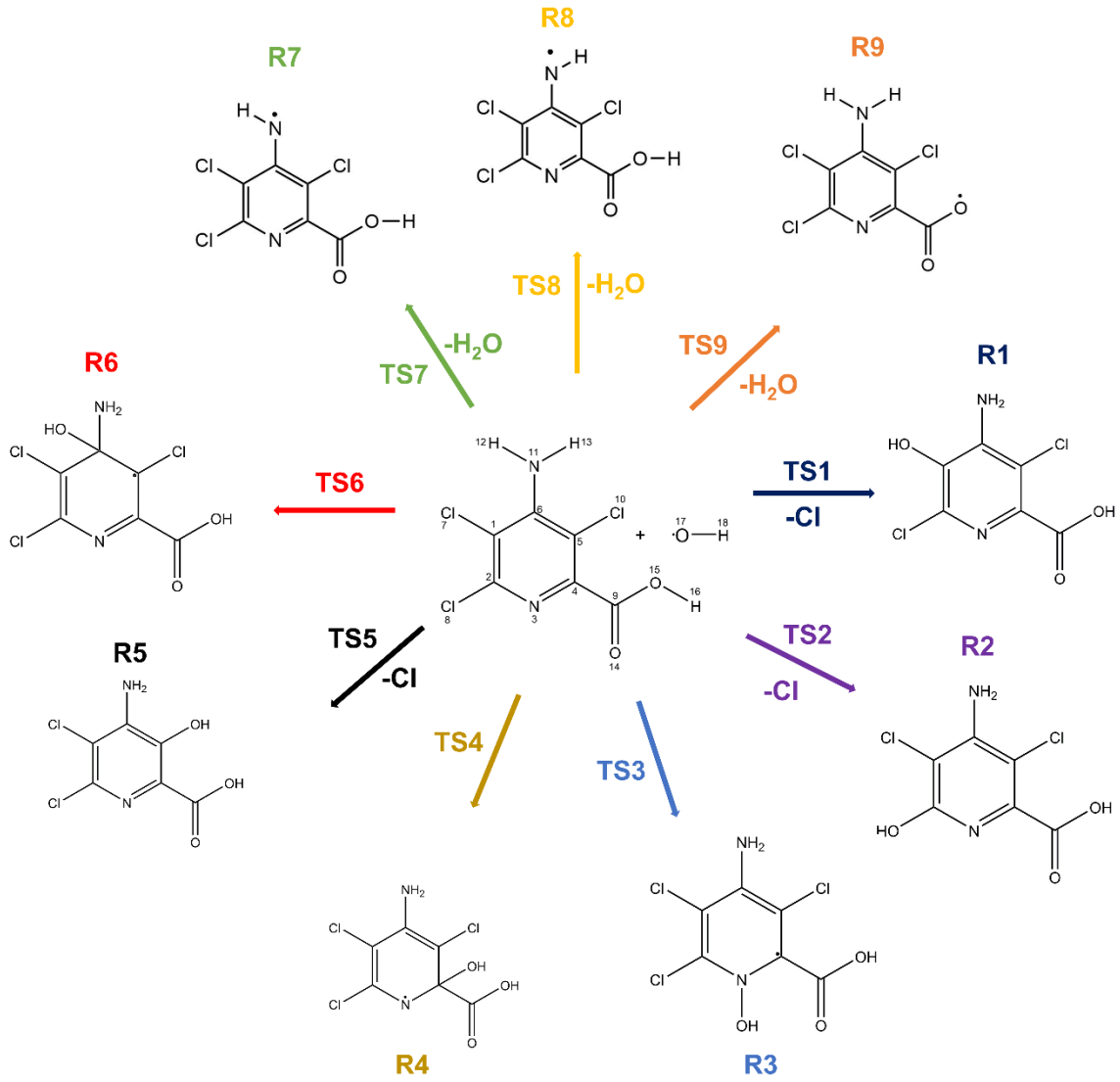

Figure 1: Scheme of hydrogen atom abstraction and addition reactions with picloram and •OH radicals.

2. Materials and Methods

2.1 Quantum chemical calculations

The electronic structure properties of the reactants, products, and the transition states were calculated at the M06HF/6-31G+(d) level (for appropriate nomenclature see Figure 1) with the solvation model density (SMD). The SMD model has been widely used to simulate the aqueous environment in the elucidation of the mechanisms of pesticide degradation, and is computationally less demanding than other continuum models (Luo et al., 2018). Details about other levels of calculations can be found in the Electronic Supplementary Information (ESI) file. The stationary points were characterized by analytic harmonic frequency calculations. The absence or presence of one imaginary frequency characterizes the optimized structures as local minima or transition states, respectively. The zero-point vibrational energy contributions have been considered in the calculation of the energy barrier. The photolysis of the optimized geometries was performed by TD-DFT (Gross et al., 1996) calculations using the CAM-B3LYP density functional (Yanai et al., 2004) and 6-311++G(d,p) basis set. Quantum chemical calculations were carried out using the Gaussian 16 package.(Frisch et al., 2016)

The topological analysis (Bader, 1985; Matta and Boyd, 2007) was performed in terms of electron density (ρ), Laplacian of electron density ($\nabla^2\rho$), Lagrangian kinetic energy density [G(r)], Potential energy density [V(r)] and Energy density [E(r)] at the Critical Points (CP) to efficiently describe H-bonding and its concept without

136 border. To analyze the main reactive sites of the•OH + picloram reaction, appropriate
137 local reactivity descriptors as Fukui function (f) (López and Méndez, 2004; Melin et
138 al., 2007) were calculated according to equations $f_{NBO}^{+} \approx \rho_{NBO}^{HOMO} = \sum_i |c_i|_{HOMO}^2$,
139 $f_{NBO}^{-} \approx \rho_{NBO}^{LUMO} = \sum_i |c_i|_{LUMO}^2$, and $f_{NBO}^{0} \approx f_{NBO}^{+} + f_{NBO}^{-}\,/2$. The Multiwfn
140 package program (Lu and Chen, 2012) was used to study the topological and Fukui
141 functions.

142 2.2 Reaction Rate Theory

143 The reaction rate constant of picloram degradation by •OH radicals was
144 calculated using formulations based on the Transition State Theory. To account for
145 the tunneling effect, the *deformed* Transition State Theory ($d-TST$) (Carvalho-Silva
146 et al., 2017) was adopted (Eq. 1):

$$k_{d-TST} = \frac{k_B T}{h}\frac{Q_{TS^{\dagger}}}{Q_{Reac}}\left(1 - d\frac{E_0}{RT}\right)^{1/d} \quad (1)$$

147 where h is the Planck's constant, k_B is the Boltzmann constant, R is the universal gas
148 constant, d is the deformation parameter, while Q_{Reac} and $Q_{TS^{\dagger}}$ are the partition
149 functions of the reactants and transition state, respectively. To include the contribution of
150 molecular diffusion in solution, the calculated rate constant k_{d-TST} is combined
151 with the steady-state Smoluchowski rate constant, k_D , following the
152 Collins-Kimball theory (Collins and Kimball, 1949), yielding the apparent rate
153 constant (k_{OBS}), according to Eq. 2:

$$\frac{\mathbf{1}}{\boldsymbol{k_{OBS}}} = \frac{\mathbf{1}}{\boldsymbol{k_{d-TST}}} + \frac{\mathbf{1}}{\boldsymbol{k_D}} \quad (2)$$

Additional details about the parameter d and the calculation of k_D can be found elsewhere (Sanches-Neto et al., 2020) and the references therein. To consider the effect of recrossing on the reaction rate constant, we also calculate the Variational Transition State Theory (VTST) (Eq. 3):

$$k_{VTST}(T) = \min_q k_{TST}(T). \quad (3)$$

However, VTST neglects tunneling effects, since it underestimates the kinetic constant for reactions where quantum tunneling effects are important, especially at low temperatures. Here, in order to account for the quantum tunneling effect, we refine the *deformed* formalism described in (Carvalho-Silva et al., 2017), defining the *deformed* Variational Transition State Theory (d-VTST) (Eq. 4):

$$k_{d-VTST}(T) = \min_q k_{d-TST}(T). \quad (4)$$

The Aquilanti-Mundim law (Aquilanti et al., 2010) (Eq. 5) was used to fit the rate constant data to represent our results in order to compare with other works:

$$k(T) = A\left(1 - \frac{\bar{d}\bar{E}}{RT}\right)^{1/\bar{d}}, \quad (5)$$

where A and $\bar{d}$ are the pre-exponential factor and the deformed parameter, respectively [Note a change in the notation here, needed in order to avoid ambiguities: in terms of the fitted equation, we defined $\bar{d}$, which is different from the d parameter; and $\bar{E}$, which is different from E_0]. All kinetic and associated parameters have been calculated with the Transitivity Code-version 1.0.4 (Machado et al., 2019). Details of the computational program can be found on the www.vhcsgroup.com/transitivity web page.

172 *2.3* Experimental approach

173 The overall second-order reaction rate constant between picloram (PCL) and •OH
174 radicals ($k_{PCL,\bullet OH}$) was evaluated using the competition kinetics method with
175 correction for photolysis, as reported elsewhere (Lastre-Acosta et al., 2019; Shemer
176 et al., 2006; Silva et al., 2015; Son et al., 2020; Wenk et al., 2011; Yan et al., 2021).
177 In this method, the rate constant is evaluated as a function of its observed
178 pseudo-first-order rate in the presence of a competing •OH radical scavenger with
179 known kinetics (p-chlorobenzoic acid, *p*CBA), according to Eqs. 7 and 8:

$$k_{PCL,\bullet OH} = \left(\frac{k_{PCL}(\text{obs}) - k_{PCL}(\text{dp})}{k_{pCBA}(\text{obs}) - k_{pCBA}(\text{dp})}\right) \times k_{pCBA,\bullet OH} \quad (6)$$

180 where k_{PCL}(obs) is the measured pseudo-first-order reaction rate of picloram in the
181 •OH radical system (described below); k_{PCL}(dp) and k_{pCBA}(dp) are the measured
182 photolysis rate constants of picloram and p-chlorobenzoic acid. k_{pCBA}(obs) and
183 $k_{pCBA,\bullet OH}$ are, respectively, the measured pseudo-first-order reaction rate constant of
184 the reference compound in the •OH radical system and the second-order rate constant
185 of the reaction between this compound and hydroxyl radicals ($k_{pCBA,\bullet OH}$ = 5 × 10^9 L
186 mol^{-1} s^{-1}) (Elovitz and Von Gunten, 1999).

187 The reactional system used in this experiment adopts hydrogen peroxide as a
188 precursor of •OH radicals. A reaction mixture is prepared containing 2.1 × 10^{-5} mol
189 L^{-1} of picloram (ca. 5 ppm), an equimolecular amount of *p*CBA (ca. 3.2 ppm) and
190 excess (0.05 mol L^{-1}) hydrogen peroxide in natural pH (~ 4.5). H_2O_2 was added in
191 excess to ensure that the competing reactions will be limited by the concentration of

the target and the reference compounds. According to the literature, the concentration of hydrogen peroxide was shown not to affect significantly the value of the second-order rate constant of the target compound with •OH radicals (Shemer et al., 2006). The test solution was prepared using deionized, ultrapure water (Milli-Q®, 18.2 MΩ), and distributed into 2.0-mL Pyrex vials with no headspace. The vials were irradiated under simulated sunlight with standard AM1.5G spectra (PEC-L01, Peccell Inc.), as illustrated in Figure 2, for selected exposure times. Samples were irradiated for 5, 10, 15, 30, 45, 60 and 120 min. All chemicals, HPLC grade, were acquired from Sigma-Aldrich and used as received without further purification.

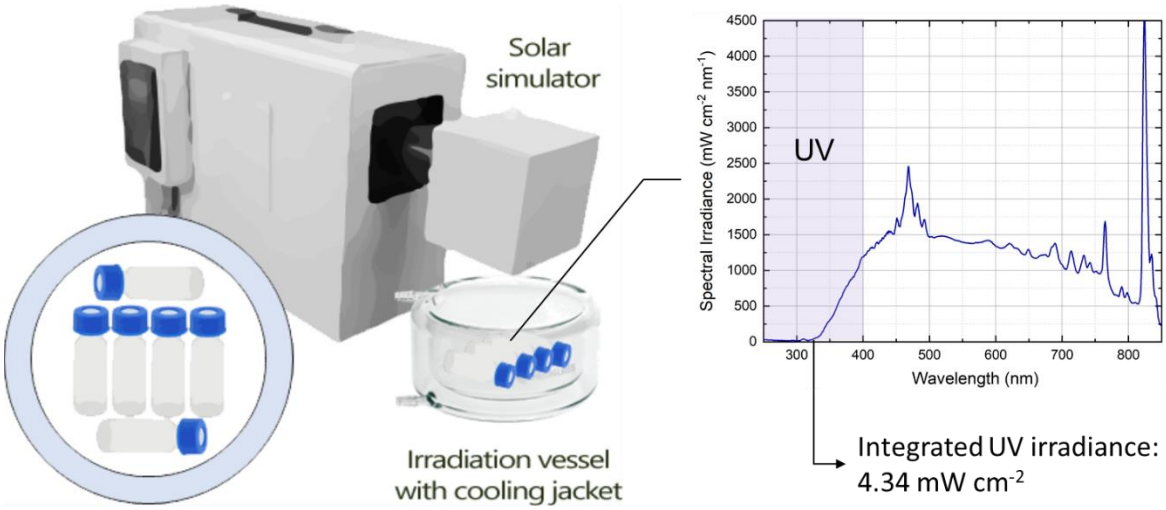

Figure 2: Illustration of the setup used in the competition kinetics and photolysis experiments.

The (direct) photolysis rate constants, k_{PCL}(dp) and k_{pCBA}(dp), are evaluated in the same experimental setup, in order to account for the effects of the irradiated photons on the degradation of both species due to excited-state reactions. However, in these

208 analyses, the sample vials are filled with solutions of each compound (5 ppm for
209 picloram and 10 ppm for pCBA) separately and without the addition of H_2O_2. The
210 concentrations of pCBA and picloram were measured using a high-precision liquid
211 chromatography system (LC-10, Shimadzu Co.) equipped with a photodiode array
212 detector (SPD-20MA, Shimadzu Co.). The separation was carried out in a C18
213 reverse-phase column (Luna C18, 5 µm, 250 × 4.6mm, Phenomenex Inc.) with
214 isocratic elution of methanol and water (50:50) at 1.5 mL min^{-1}. Picloram and *p*CBA
215 were detected simultaneously after 4.7 and 13.7 min of elution, respectively, and
216 quantified by UV absorption at 254 nm.

217 *2.4* Toxicity assessment

218 The ecotoxicity of picloram and its main degradation products were determined
219 using the Ecological Structure-Activity Relationship Model (ECOSAR V2.0).
220 ECOSAR is an effective predictive program and has been successfully applied to the
221 ecotoxicity assessment of organic contaminants (Reuschenbach et al., 2008;
222 Sanderson et al., 2003). Three aquatic organisms – green algae, daphnia, and fish –
223 were chosen as targets. Acute toxicity (feature characterized by LC_{50} and EC_{50}
224 values) and chronic toxicity (defined by ChV) of the compounds studied were
225 obtained from ECOSAR platform. LC_{50} means the concentration of a chemical
226 compound (in mg L^{-1}) that causes the death of half of the fish and daphnia
227 population after exposures of 96 and 48 h, respectively. In addition, EC_{50} represents
228 the concentration that permits 50% of green algae to grow normally after 96 h of
229 exposure (in mg L^{-1}).

3. Results and Discussion

3.1 Experimental

The first-order degradation profiles of picloram and *p*CBA in the hydroxyl radical reaction system are shown in Figure 3. Both profiles adjusted well to a first-order kinetics, according to Eqs. 7 and 8:

$$\ln\left(\frac{C_0(PCL)}{C(PCL)}\right) = k_{PCL}(obs)\ \ t_{irrad} \quad (7)$$

$$\ln\left(\frac{C_0(pCBA)}{C(pCBA)}\right) = k_{pCBA}(obs)\ \ t_{irrad} \quad (8)$$

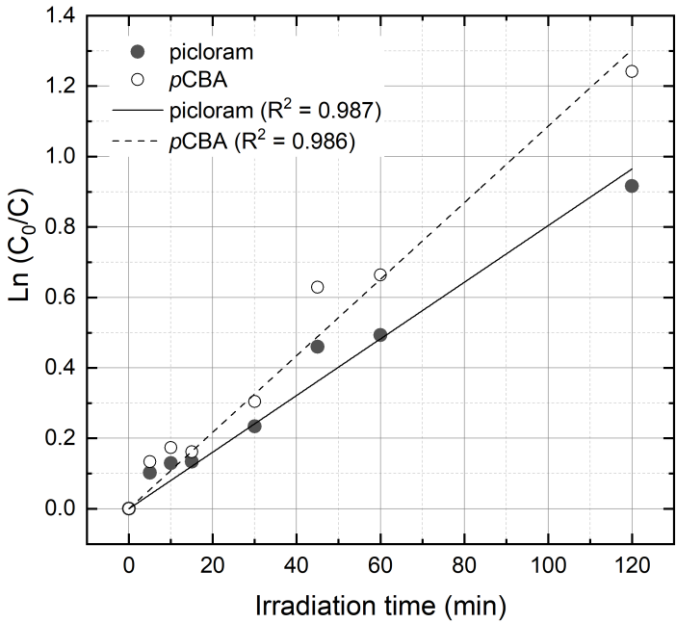

Figure 3: Pseudo-first-order plots of picloram and pCBA in the hydroxyl radical reaction system.

The reaction rate constants evaluated at this stage are used to calculate $k_{PCL,\bullet OH}$, together with the reaction rates evaluated in the absence of H_2O_2, in order to exclude

241 the effects of direct photolysis, as indicated in Eq. 6. Table 1 summarizes the kinetic
242 constants measured experimentally.

243 **Table 1**: Kinetic parameters obtained experimentally.

Rate constant		Picloram
Direct photolysis	k_{PCL}(dp)	$(2.71 \pm 1.95) \times 10^{-6}$ s^{-1}
$^{\bullet}$OH (pseudo first-order)	k_{PCL}(obs)	$(1.30 \pm 0.04) \times 10^{-4}$ s^{-1}
Second-order	$k_{PCL,^{\bullet}OH}$	$(6.74 \pm 0.13) \times 10^{-12}$ cm^3 $molecules^{-1}$ s^{-1}

244 The second-order reaction rate constant is within the range commonly found for
245 the reaction of aromatic compounds and pyridines with hydroxyl radicals (Buxton et
246 al., 1988), typically between 8.0×10^{-13} and 2.5×10^{-11} cm^3 $molecules^{-1}$ s^{-1}. Özcan and
247 colleagues (Özcan et al., 2008) have carried out a similar competitive kinetics
248 experiment for picloram and reported a second-order rate constant in the same order of
249 magnitude, albeit slightly slower than ours (5.64×10^{-12} cm^3 $molecules^{-1}$ s^{-1}). This
250 difference is expected, since our reactive media are substantially different, particularly
251 in terms of pH. As shown in Buxton's comprehensive database of kinetic constant
252 rates of organic species with oxygen radicals (Buxton et al., 1988), the measured
253 reaction rates can vary within the same order of magnitude for similar organic
254 compounds according to the reaction pH. Considering the reported pKa of picloram
255 (3.4) (Spadotto and Hornsby, 2003), it is expected that at natural pH most picloram
256 molecules will be in the ionic state; whereas at a pH 3.0, the condition used by Özcan,
257 most of their equivalents would be in the neutral molecular form.

3.2 Mechanism and energetic parameters

To discuss the mechanisms of the reaction of •OH radicals with picloram, we used the M06HF density functional, which is widely used to study chemical reactions and provides a reliable mechanism and kinetic results (Sanches-Neto et al., 2020; Sanches-Neto et al., 2017), combined with the 6-31+G(d) base function. Additional calculations with larger basis sets and other DFT functionals were considered, whose results are shown in Table S1. The possible mechanisms for the reaction of •OH radicals with picloram are (see nomenclature in Figure 1): i) hydrogen transfer from the amino group (R7-R8) or carboxylic group (R9) of picloram by the •OH radical and/or ii) •OH addition to the picloram pyridinic ring (R1-R6). In this study, the single-electron transfer mechanism (SET) is not considered because the barrier height of SET is higher than the reactions involving abstraction and addition (Han et al., 2014; Li et al., 2020; Yang et al., 2017). To confirm the main active sites of the picloram molecule through radical attack, the Fukui functions were calculated, an important approach to explain the reactivity in chemical systems (López and Méndez, 2004; Melin et al., 2007; Milenković et al., 2020; Silva et al., 2010). Figure 4 illustrates significant values (see nomenclature in Figure 1) for the selected atoms. According to Fukui formulation (López and Méndez, 2004), the highest values are related to a probable radical attack on carbon C1, C4, and C5.

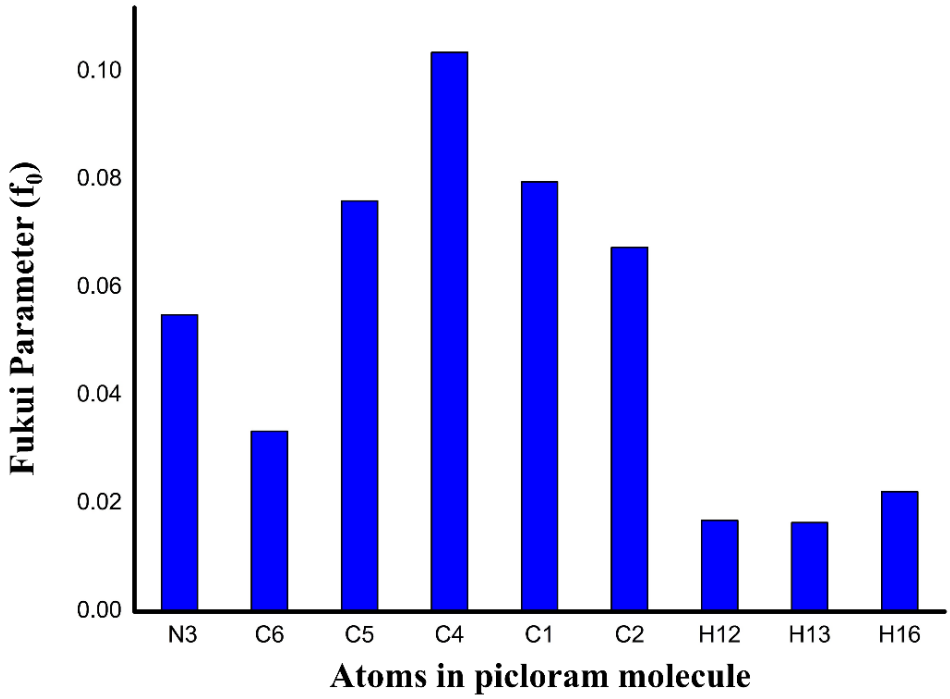

276

277 **Figure 4**: Fukui function values for the •OH radical attack on selected carbon atoms of
278 picloram in water (see nomenclature in Figure 1).

279 Figure 3 shows the relative energy profile of the reaction of picloram with •OH
280 radicals calculated at the M06HF/6-31+G(d) level of theory and corroborates the
281 results of the Fukui function – the attack of the •OH radicals on carbons C1, C4, and
282 C5 is kinetically favorable: R1, R4, and R5 channels presented the lowest barrier
283 heights. The Cartesian coordinates of the transition states and picloram calculated in
284 this work are listed in Table S2. Geometric parameters and imaginary frequencies of
285 the transition states involved in the reaction of •OH radicals with picloram are listed
286 in Table S3. From the data in Table S3, it is possible to observe that the transition
287 state geometries for R1 and R5 channels are similar: at the M06HF/6-31+G(d) level,
288 we found the C_1-O_{17}-H_{18} and C_5-O_{17}-H_{18} angles of 102.88° and 95.66° and the
289 frequency values for TS1 and TS5 of 650.13*i* and 681.27*i*, respectively; this

information is very important in modeling the global potential energy surface for future calculations (Truong et al., 1989). The thermodynamic profile of all the pathways presented in Figure 1 (R1-R9) was studied and revealed that only the R3 channel is endothermic. The formation of R1, R2, and R5 products occurs by addition of the •OH radical to the picloram ring, forming an intermediate, followed by reductive elimination of the chlorine atom (Abramović et al., 2011; Özcan et al., 2008). The R5 product (4-amino-2,3-dichloro-5-hydroxy-picolinic) has also been reported by previous studies (Abramović et al., 2011; Coledam et al., 2018; Özcan et al., 2008; Rahman and Muneer, 2005).

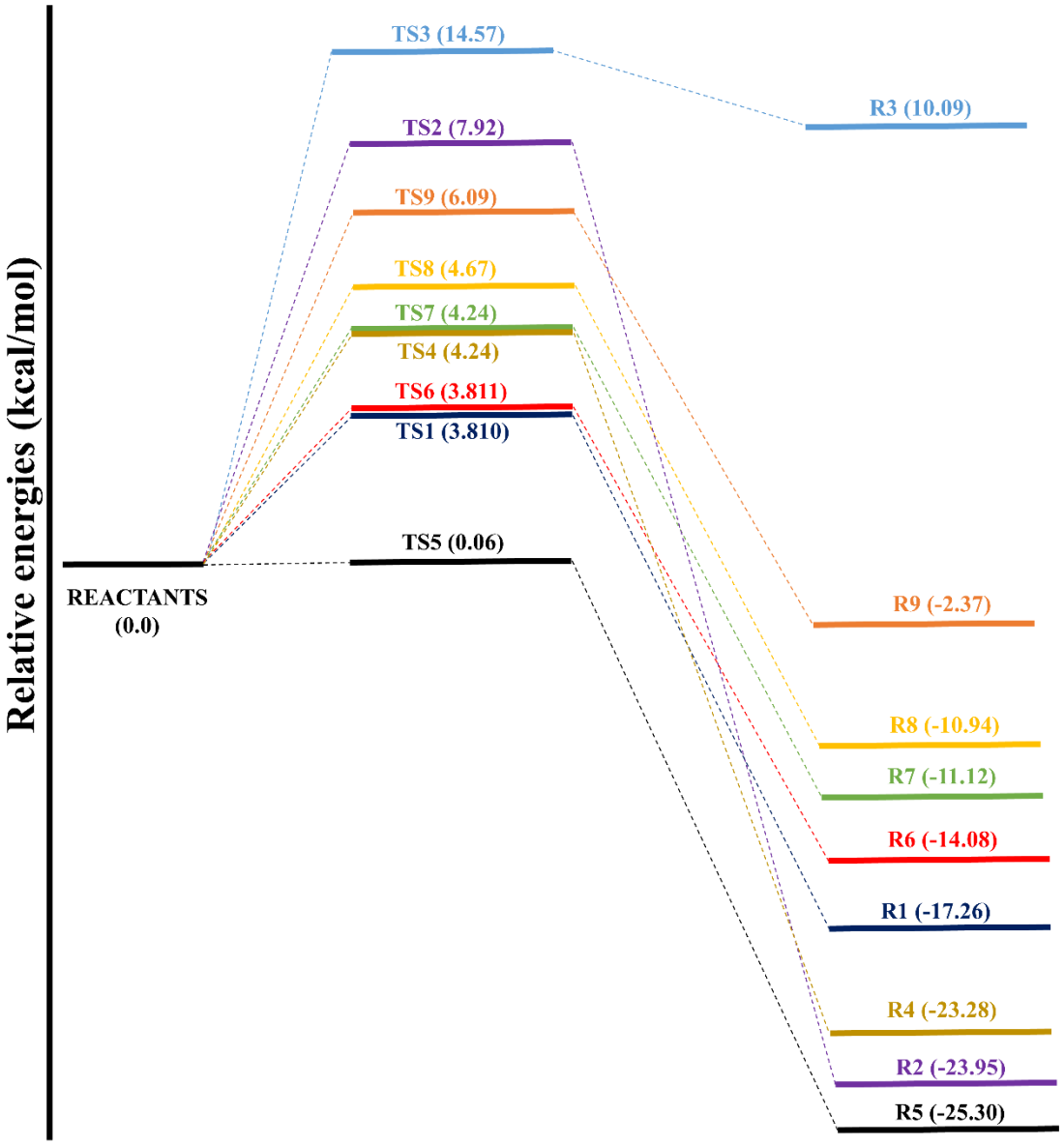

Figure 5: Relative energy profile corresponding to the initial abstraction of the hydrogen atom and picloram addition reaction by the •OH radical.

Additionally, we make use of the Quantum Theory of Atoms in Molecules (QTAIM) to explain the strong thermodynamic stability of R1 and R5 products from their intermolecular interaction. These products are the major degradation compounds found experimentally (see more details in Sec. 3.3). According to Rozas' (Rozas et al., 2000) criteria, intermolecular interactions can be classified as:

307 strong, when $\nabla^2\rho(r) < 0$, $E(r) < 0$, and $|V(r)| > E(r)$; ii) weak, when $\nabla^2\rho(r) > 0$, and
308 $E(r) > 0$; and iii) moderate, when $\nabla^2\rho(r) > 0$, and $E(r) < 0$. According to Table 2,
309 there is a strong hydrogen bond between H_{18} of the hydroxyl group and O_{15} of the
310 carboxylic group permitting an efficient stabilization of the R5 product. Cl_{10} in the
311 R1 product provokes a concomitant stabilization mediated by H_{15} and O_{17} atoms.
312 Molecular representations of critical points (CP) shown in Table 2 are in Figure S1
313 of ESI.

314 **Table 2**: Topological parameters of critical point density, calculated at the theory level
315 M06HF/6-31+G(d) for R1 and R5 products. The parameters $\rho(r)$, G(r), V(r), E(r) and
316 $\nabla^2\rho(r)$ are in atomic units.

Interaction	Product	$\rho(r)$	G(r)	V(r)	E(r)	$\nabla^2\rho(r)$
Cl_{10}-O_{17}	R1	0.01270	0.01037	-0.00155	-0.00882	0.001548
Cl_{10}-H_{13}	R1	0.01607	0.01442	-0.00304	-0.01137	0.003045
H_{18}-O_{15}	R5	0.04136	0.03584	0.00273	-0.03856	-0.00273

317 *3.2 Theoretical reaction rate constant*

318 Several authors have suggested that the reductive elimination steps after the
319 addition of the •OH radical are not determinant for the calculation of the rate
320 constant (Abramović et al., 2011). Accordingly, reaction rate constants calculated in
321 the present study considered only •OH radical additions in the picloram ring and
322 hydrogen abstraction from the amino and carboxylic groups. To the best of our

knowledge, these are the first theoretical calculations of the reaction rate constant of picloram degradation mediated by •OH radicals.

First, the reaction rate constants of picloram were calculated using the *deformed* Transition State Theory (*d*-TST) in a realistic temperature range (250.0-310.0 K) at the M06HF/6-31+G(d) level. The results are presented in Table 2. The value of the total reaction rate constant at 298.15 K is 4.29×10^{-12} $cm^3 \cdot molecules^{-1} \cdot s^{-1}$, which is in excellent agreement with the value found experimentally in this work and by Özcan et al (Özcan et al., 2008), 4.53×10^{-12} cm^3 $molecules^{-1}$ s^{-1}. It is observed that the temperature dependence of the reaction rate constants of picloram degradation by •OH attack exhibits anti-Arrhenius behavior – a decrease in the reaction rate constant as the temperature increases. Previous studies have shown that reactions with hydroxyl radicals often exhibit deviations from the Arrhenius law. For cases with anti-Arrhenius behavior, the reactional process is characterized by a stereodirectional factor (Coutinho et al., 2018, 2016, 2015). These findings clarify the favoring of the attack of the •OH radical to C5 of picloram. The substitution of an electron-withdrawing group (Cl) by an electron-donating group (•OH) results in a strong stabilization due to the OH-H18 hydrogen bond with the R5 product. These observations support the role of the orientational factor in this reaction.

Recently, we developed a web application structured in a machine learning and molecular fingerprint algorithm for the estimation of the reaction rate constants of the degradation of organic pollutants in aqueous environments - the *pySiRC* platform

(www.pysirc.com.br) (Sanches-Neto et al., submitted.). Table 3 shows the reaction rate constant estimated by the Bagging machine learning (ML) model in pySiRC. There is an excellent agreement between our quantum chemistry protocol and the ML algorithm.

Table 3: Reaction rate constants of picloram degradation by ˙OH attack calculated at the M06HF/6-31+G(d) level with the SMD continuous solvation model using $\boldsymbol{d}$-TST formulation. Units in $cm^3 \cdot molecules^{-1} \cdot s^{-1}$.

Rate constant	Temperature (K)				
	250.0	273.15	298.15	300.0	310.0
$\boldsymbol{k_{R1}}$	2.14×10^{-12}	1.98×10^{-12}	1.84×10^{-12}	1.83×10^{-12}	1.79×10^{-12}
$\boldsymbol{k_{R2}}$	6.84×10^{-19}	2.28×10^{-18}	6.84×10^{-18}	7.37×10^{-18}	1.09×10^{-17}
$\boldsymbol{k_{R3}}$	6.18×10^{-25}	6.02×10^{-24}	4.77×10^{-23}	5.49×10^{-23}	1.14×10^{-22}
$\boldsymbol{k_{R4}}$	8.95×10^{-16}	1.53×10^{-15}	2.52×10^{-15}	2.61×10^{-15}	3.12×10^{-15}
$\boldsymbol{k_{R5}}$	2.77×10^{-12}	2.59×10^{-12}	2.45×10^{-12}	2.44×10^{-12}	2.39×10^{-12}
$\boldsymbol{k_{R6}}$	1.04×10^{-17}	2.53×10^{-17}	5.72×10^{-17}	6.05×10^{-17}	8.07×10^{-17}
$\boldsymbol{k_{R7}}$	3.85×10^{-18}	1.01×10^{-17}	2.50×10^{-17}	2.66×10^{-17}	3.69×10^{-17}
$\boldsymbol{k_{R8}}$	1.89×10^{-18}	4.75×10^{-18}	1.130×10^{-17}	1.20×10^{-17}	1.65×10^{-17}
$\boldsymbol{k_{R9}}$	6.52×10^{-22}	3.11×10^{-21}	1.35×10^{-20}	1.49×10^{-20}	2.52×10^{-20}
This work (Theoretical/$\boldsymbol{k_{Total}}$)	4.92×10^{-12}	4.57×10^{-12}	4.29×10^{-12}	4.27×10^{-12}	4.18×10^{-12}
Özcan			4.53×10^{-12}		
pySiRC			4.13×10^{-12}		
This work (Experimental)			6.74×10^{-12}		

The branching ratios (Γ_j) were calculated, defined as the ratio of the rate constant of a specific channel and the global rate constant for each channel ($\Gamma_j = k_j/k_{Total}$). The values of the major contributions are given in Table 4, and the results indicate the preference for channels R1 and R5 with branching ratios of 42.9% and 57.1%, at 298.15 K, respectively. The knowledge of the effective importance of each channel

is significant and allows the role played by each of these products in the environment to be evaluated.

Table 4: Branching ratios, in %, of the elementary channels of picloram degradation using d-TST calculated at the M06HF/6-31+G(d) level of theory.

Branching ratio	Temperature (K)				
	250.0	273.15	298.15	300.0	310.0
Γ_{R1}	43.60	43.30	42.90	42.80	42.80
Γ_{R4}	0.018	0.034	0.059	0.061	0.075
Γ_{R5}	56.40	56.70	57.10	57.10	57.10

The reaction rate constant (k_{OBS}) were corrected using the Collins-Kimball formulation to account for diffusion effects. The values of the total diffusion constant (k_D) of the reaction are one or two orders of magnitude higher than the reaction rate constants of R1 and R5 channels (see Table S4), which is within the activation-controlled limit; hence, the reaction rate constant is determined by the elementary rate constant. For reactions with energy barrier values close to zero, it is recommended to use the Variational Transition State Theory (VTST) (Bao and Truhlar, 2017; Zhang et al., 2020). Here, we calculated the reaction of the $^{\bullet}$OH radical with picloram for the majority R1 and R5 channels using VTST. For the first time, we also applied the variational correction in the d-TST formulation to correct errors due to crossover. The values of the rate constant using the variational correction of TST and d-TST, in the range 250.0-310 K are presented in Table S4.

To evaluate the total reaction rate constant of picloram with •OH radicals, we adjusted the temperature dependence using the Aquilanti-Mundim law, which has been used successfully to describe the kinetics of chemical processes (Coutinho et al., 2016, 2015) (see Table S5). The profile of equations fitted to Table S5 in the Arrhenius plot showed negative activation energy (anti-Arrhenius kinetics).

From the data of the total reaction rate constant of picloram with the •OH radical obtained by $\mathcal{A}$-TST, it is possible to calculate the half-life time using $t_{1/2} = ln2\ /(k_{total} \times [\bullet OH])$, where $[\bullet OH]$ is the concentration of •OH radicals in the aqueous media. The half-life of the reaction was studied in the temperature range 273.15-310 K, and $[\bullet OH]$ 10^{-15}-10^{-18} mol L^{-1}, which usually represents the values found in surface waters (Brezonik and Fulkerson-Brekken, 1998; Burns et al., 2012; J. Yang et al., 2020). The calculated half-lives are shown in Figure 4. From our results, the half-life varies from 31 to 310 days considering a concentration of •OH radicals in the range 10^{-16}-10^{-17} mol L^{-1}, respectively. Our theoretical values are in agreement with the results obtained experimentally, which report a lifetime in the range of 20 to 300 days (Özcan et al., 2008; Wauchope et al., 1992).

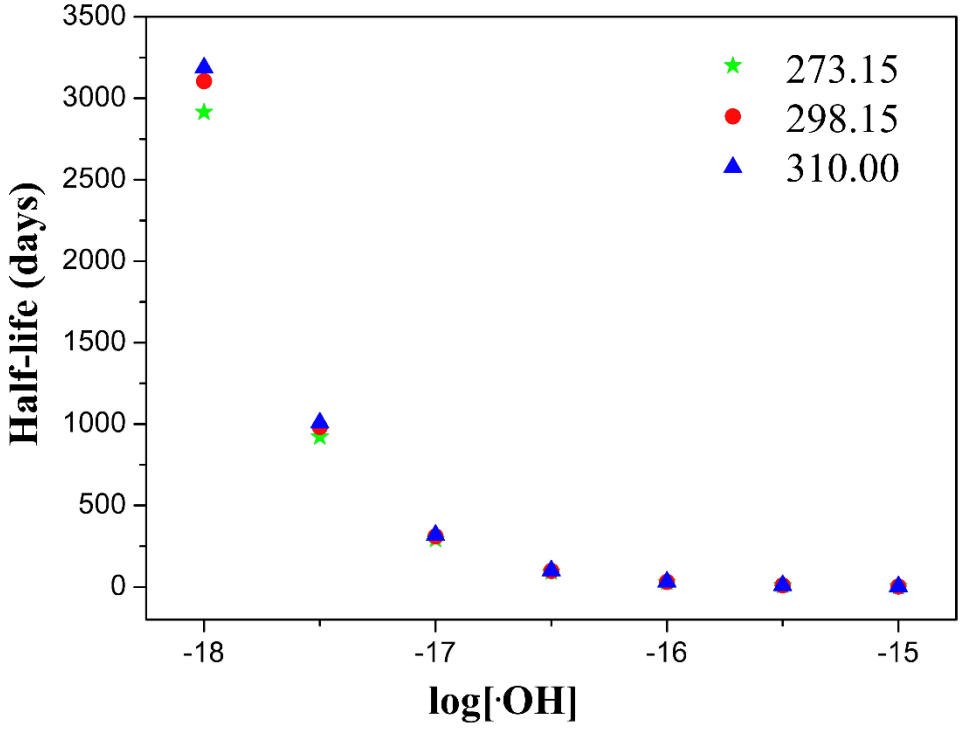

388

389 **Figure 6**: Half-life time, in days, of picloram degradation as a function of •OH
390 concentration, in mol L^{-1}, in the temperature range 273.15-310 K in natural waters.

391 3.3 Toxicity evaluation

392 Many studies that have applied AOPs to remove pesticides showed products
393 with toxicity higher than the parent compound (Manonmani et al., 2020, 2019).
394 Computer programs based on an ecological structure-activity relationship model
395 have been widely used to evaluate the environmental and health risks that
396 degradation products might pose. In this work, the toxicity of picloram and the main
397 by-products generated through •OH attack were evaluated using the ECOSAR
398 program (Mei et al., 2019; Milenković et al., 2020; J. Yang et al., 2020). Table 5
399 shows the toxicity classification according to the criteria established by the European
400 Union and China for acute toxicity (LC_{50} or EC_{50}) and chronic toxicity (ChV).

Table 5: Classification of acute and chronic toxicity according to the criteria established by the European Union and Chinese Regulations.

Classification	Acute toxicity[a]	Chronic toxicity[b]
Not harmful	$LC_{50} > 100$ or $EC_{50} > 100$	ChV > 10
Harmful	$10 < LC_{50} < 100$ or $10 < EC_{50} < 100$	1 < ChV < 10
Toxic	$1 < LC_{50} < 10$ or $1 < EC_{50} < 10$	0.1 < ChV < 1
Very toxic	$LC_{50} < 1$ or $EC_{50} < 1$	ChV < 0.1

[a] Criteria set by the European Union (described in Annex VI of Directive 67/548/EEC)

[b] Criteria set by the Chinese hazard evaluation guidelines for new chemical substances (HJ/T 154–2004)

The estimated toxicities of the compounds to fish, daphnia, and green algae are reported in Table 6. According to the toxicity parameters, the degradation of picloram via the R1 channel leads to a less toxic product. On the other hand, the R5 product presents higher acute and chronic toxicities than picloram. Recent work evaluating the sulfate-radical oxidation of picloram presented similar toxicity results for picloram and its degradation products (Yang et al., 2020). Interestingly, the R1 and R5 products were not detected when the degradation was carried out with the $SO_4^{\bullet-}$ radical. These results reinforce the need to continue the research on the chain of reactions involved in these complex systems to elucidate the main mechanisms of picloram degradation in radical-based AOPs.

Table 6: Toxicity of picloram and its main by-products generated through •OH radical attack.

Organisms	Compounds		
	picloram	R1	R5
LC_{50} (fish 96 h)	13.55	3410	568.0
LC_{50} (daphnia 48 h)	1.82	65.60	32.40
EC_{50} (green algae 96 h)	1.18	232.0	93.40
ChV (fish, chronic)	0.55	70.90	7.230
ChV (daphnia, chronic)	0.17	0.680	0.376
ChV (green algae, chronic)	0.43	132.0	32.30

3.4 Photolysis

The toxicity analysis discussed in the previous section shows that the main by-products can be considered harmful. In order to evaluate an alternative degradation pathway, the photolysis of picloram and its major products was performed using the (TD)CAMB3LYP/6-311++G(d,p) level of calculation, which is widely used to study chemical reactions in the excited state (Kayanuma et al., 2019). Table 7 shows the excitation energy, absorption wavelength, and strength of the harmonic oscillator for picloram and R1 and R5 products.

Table 7: Vertical excitation energy (eV), absorption wavelength (nm) and oscillator strength (a.u) of picloram and R1 and R5 by-products calculated at the TD-CAM-B3LYP/6-311++G(d,p) level of theory.

Compouds	Excitation energy	Wavelength	Oscillator strength
Picloram	5.4581	227.16	0.8840
R1	5.2080	238.06	0.3774
R5	3.8734	320.09	0.2576

Vertical excitation energies smaller than 4.13 eV (~ 300 nm) indicate that the compounds may undergo photolysis under sunlight (Bai et al., 2015). From Table 7, both picloram and the R1 product will not photolyze at room temperature. However, the R5 product – the most thermodynamically favorable reaction product but with higher toxicity levels than picloram – may undergo photolysis. Figure 7 shows the simulated absorption spectra of picloram, with an absorption peak (227 nm) in agreement with experimental observations (223 nm), as well as other degradation products (Dos Santos et al., 2010). A complementary analysis of the bond distances of the R5 product in the ground and first excited state was performed. The values of these optimized parameters are listed in Table S6. Note that the hydrogen bond (H18…O15) decreases by 0.25 Å, suggesting a possible intramolecular transfer of protons in the excited state. These results show the need for a better understanding of subsequent reactions of hydroxyl radical-based oxidation in aqueous solution.

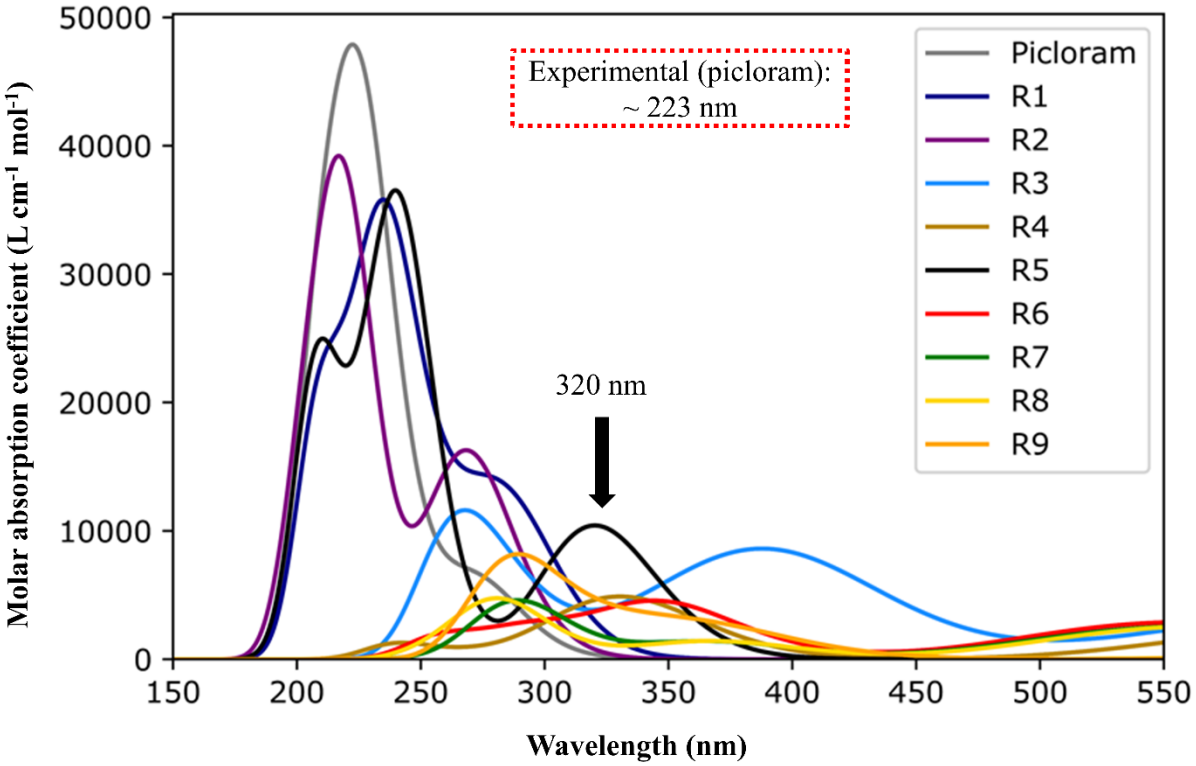

443

444 **Figure 7:** UV-VIS absorption spectra of picloram and degradation by-products calculated
445 at the (TD)CAM-B3LYP/6-311++G(d,p) level of theory. The experimental value is also
446 presented for comparison (Dos Santos et al., 2010).

447 ## 4. Conclusions

448 This work presents for the first time a theoretical study of the degradation of
449 picloram by •OH radicals in aqueous media using a blend of quantum chemistry
450 calculations and reaction rate theories. The calculated values were compared with
451 experimental data obtained by competition kinetics. The mechanisms of picloram
452 degradation and reaction kinetics are reported, and the results show that •OH
453 addition of picloram occurs favorably at the C1 and C5 sites of picloram. The
454 reaction rate constant was calculated with formulations derived from the Transition

State Theory. The predicted values for the total rate constant and half-life time at 298.15 K are in very good agreement with experimental results. From the elementary reaction rate constants, the branching ratios of each channel were calculated, accounting R1 and R5 channels as the major by-products. An analysis of the toxicity of picloram and R1 and R5 by-products was performed with the ECOSAR program, showing that these compounds are harmful to living organisms. A photolysis assessment of picloram and R5 by-product indicates that these intermediates can easily be sensitized in sunlight, suggesting additional degradation routes.

Author Contributions: All authors contributed equally to the planning of the research and the writing of the paper.

Conflict of Interest: The authors declare that the research was conducted in the absence of any commercial or financial relationships that could be construed as a potential conflict of interest.

Acknowledgments: The authors acknowledge the Brazilian funding agencies Coordenação de Aperfeiçoamento de Pessoal de Nível Superior (CAPES) (Finance Code 001), the National Council for Scientific and Technological Development (CNPq, Brazil), and the support of the Sao Paulo Research Foundation (FAPESP Grants 2019/24158-9 and 2018/21721-6) and the Goias State agency FAPEG for the research funding programs (AUXÍLIO À PESQUISA COLABORATIVA FAPEG-FAPESP/GSP2019011000037). This research is also supported by the High-Performance Computing Center at the Subsecretaria de Tecnologia da Informação (STI), in the Secretaria de Desenvolvimento e Inovação (SEDI), Brazil.

References

Abramović, B., Šojić, D., Despotović, V., Vione, D., Pazzi, M., Csanádi, J., 2011. A comparative study of the activity of TiO2 Wackherr and Degussa P25 in the photocatalytic degradation of picloram. Appl. Catal. B Environ. 105, 191–198.

An, T., Gao, Y., Li, G., Kamat, P. V., Peller, J., Joyce, M. V., 2014. Kinetics and mechanism of •oH mediated degradation of dimethyl phthalate in aqueous solution: Experimental and theoretical studies. Environ. Sci. Technol. 48, 641–648.

Aquilanti, V., Mundim, K.C., Elango, M., Kleijn, S., Kasai, T., 2010. Temperature dependence of chemical and biophysical rate processes: Phenomenological approach to deviations from Arrhenius law. Chem. Phys. Lett. 498, 209–213.

Bader, R.F.W., 1985. Atoms in molecules. Acc. Chem. Res. 18, 9–15.

Bai, F.-Y., Wang, X., Sun, Y.-Q., Pan, X.-M., 2015. Atmospheric chemistry of alkyl iodides: theoretical studies on the mechanisms and kinetics of CH3I/C2H5I+ NO3 reactions. RSC Adv. 5, 88087–88095.

Bao, J.L., Truhlar, D.G., 2017. Variational transition state theory: theoretical framework and recent developments. Chem. Soc. Rev. 46, 7548–7596.

Brezonik, P.L., Fulkerson-Brekken, J., 1998. Nitrate-induced photolysis in natural waters: controls on concentrations of hydroxyl radical photo-intermediates by natural scavenging agents. Environ. Sci. Technol. 32, 3004–3010.

Burns, J.M., Cooper, W.J., Ferry, J.L., King, D.W., DiMento, B.P., McNeill, K., Miller, C.J., Miller, W.L., Peake, B.M., Rusak, S.A., others, 2012. Methods for reactive oxygen species (ROS) detection in aqueous environments. Aquat. Sci. 74, 683–734.

Buxton, G. V., Greenstock, C.L., Helman, W.P., Ross, A.B., 1988. Critical Review of rate constants for reactions of hydrated electrons, hydrogen atoms and hydroxyl radicals (·OH/·O− in Aqueous Solution. J. Phys. Chem. Ref. Data 17, 513–886.

Canna-Michaelidou, S., Nicolaou, A.-S., 1996. Evaluation of the genotoxicity potential (by Mutatox™ test) of ten pesticides

found as water pollutants in Cyprus. Sci. Total Environ. 193, 27–35.

Cardoso, L.P., Valim, J.B., 2006. Study of acids herbicides removal by calcined Mg-Al-CO3-LDH. J. Phys. Chem. Solids 67, 987–993.

Carvalho-Silva, V.H., Aquilanti, V., de Oliveira, H.C.B., Mundim, K.C., 2017. Deformed transition-state theory: Deviation from Arrhenius behavior and application to bimolecular hydrogen transfer reaction rates in the tunneling regime. J. Comput. Chem. 38, 178–188.

Coledam, D.A.C., Sánchez-Montes, I., Silva, B.F., Aquino, J.M., 2018. On the performance of HOCl/Fe2+, HOCl/Fe2+/UVA, and HOCl/UVC processes using in situ electrogenerated active chlorine to mineralize the herbicide picloram. Appl. Catal. B Environ. 227, 170–177.

Collins, F.C., Kimball, G.E., 1949. Diffusion-Controlled Reactions in Liquid Solutions. Ind. Eng. Chem. 41, 2551–2553.

Coutinho, N.D., Aquilanti, V., Silva, V.H.C., Camargo, A.J., Mundim, K.C., De Oliveira, H.C.B., 2016. Stereodirectional Origin of anti-Arrhenius Kinetics for a Tetraatomic Hydrogen Exchange Reaction: Born-Oppenheimer Molecular Dynamics for OH + HBr. J. Phys. Chem. A 120, 5408–5417.

Coutinho, N.D., Sanches-Neto, F.O., Carvalho-Silva, V.H., de Oliveira, H.C.B., Ribeiro, L.A., Aquilanti, V., 2018. Kinetics of the OH+ HCl→ H2O+ Cl reaction: Rate determining roles of stereodynamics and roaming and of quantum tunneling. J. Comput. Chem. 39, 2508–2516.

Coutinho, N.D., Silva, V.H.C., De Oliveira, H.C.B., Camargo, A.J., Mundim, K.C., Aquilanti, V., 2015. Stereodynamical origin of anti-arrhenius kinetics: Negative activation energy and roaming for a four-atom reaction. J. Phys. Chem. Lett. 6, 1553–1558.

Dos Santos, L.B.O., Infante, C.M.C., Masini, J.C., 2010. Determination of picloram in waters by sequential injection chromatography with UV detection. J. Braz. Chem. Soc. 21, 1557–1562.

Elovitz, M.S., Von Gunten, U., 1999. Hydroxyl radical/ozone ratios during ozonation processes. I. The R(ct) concept.

523 Ozone Sci. Eng. 21, 239–260.

524 Frisch, M.J., Trucks, G.W., Schlegel, H.B., Scuseria, G.E., Robb, M.A., Cheeseman, J.R., Scalmani, G., Barone, V.,
525 Petersson, G.A., Nakatsuji, H., Li, X., Caricato, M., Marenich, A. V, Bloino, J., Janesko, B.G., Gomperts, R.,
526 Mennucci, B., Hratchian, H.P., Ortiz, J. V, Izmaylov, A.F., Sonnenberg, J.L., Williams-Young, D., Ding, F.,
527 Lipparini, F., Egidi, F., Goings, J., Peng, B., Petrone, A., Henderson, T., Ranasinghe, D., Zakrzewski, V.G., Gao, J.,
528 Rega, N., Zheng, G., Liang, W., Hada, M., Ehara, M., Toyota, K., Fukuda, R., Hasegawa, J., Ishida, M., Nakajima, T.,
529 Honda, Y., Kitao, O., Nakai, H., Vreven, T., Throssell, K., Montgomery Jr., J.A., Peralta, J.E., Ogliaro, F., Bearpark,
530 M.J., Heyd, J.J., Brothers, E.N., Kudin, K.N., Staroverov, V.N., Keith, T.A., Kobayashi, R., Normand, J.,
531 Raghavachari, K., Rendell, A.P., Burant, J.C., Iyengar, S.S., Tomasi, J., Cossi, M., Millam, J.M., Klene, M., Adamo,
532 C., Cammi, R., Ochterski, J.W., Martin, R.L., Morokuma, K., Farkas, O., Foresman, J.B., Fox, D.J., 2016.
533 Gaussian16 Revision C.01.

534 Ghauch, A., 2001. Degradation of benomyl, picloram, and dicamba in a conical apparatus by zero-valent iron powder.
535 Chemosphere 43, 1109–1117.

536 Gross, E.K.U., Dobson, J.F., Petersilka, M., 1996. Density functional theory of time-dependent phenomena, in: Density
537 Functional Theory II. Springer, pp. 81–172.

538 Haag, W.R., David Yao, C.C., 1992. Rate Constants for Reaction of Hydroxyl Radicals with Several Drinking Water
539 Contaminants. Environ. Sci. Technol. 26, 1005–1013.

540 Han, D., Li, J., Cao, H., He, M., Hu, J., Yao, S., 2014. Theoretical investigation on the mechanisms and kinetics of
541 OH-initiated photooxidation of dimethyl phthalate (DMP) in atmosphere. Chemosphere 95, 50–57.

542 Hedlund, R.T., Youngson, C.R., 1972. The rates of photodecomposition of picloram in aqueous systems. Adv. Chem. Ser.
543 no.111, 159–172.

544 Howard, P., 2017. Handbook of environmental fate and exposure data: for organic chemicals, volume III pesticides.

545 Routledge.

546 Ikehata, K., El-Din, M.G., 2006. Aqueous pesticide degradation by hydrogen peroxide/ultraviolet irradiation and
547 Fenton-type advanced oxidation processes: A review. J. Environ. Eng. Sci. 5, 81–135.

548 Kayanuma, M., Shoji, M., Furuya, K., Aikawa, Y., Umemura, M., Shigeta, Y., 2019. Theoretical study of the
549 photodissociation reaction of methanol. Chem. Phys. Lett. 714, 137–142.

550 Lastre-Acosta, A.M., Barberato, B., Parizi, M.P.S., Teixeira, A.C.S.C., 2019. Direct and indirect photolysis of the antibiotic
551 enoxacin: kinetics of oxidation by reactive photo-induced species and simulations. Environ. Sci. Pollut. Res. 26,
552 4337–4347.

553 Li, H., Miao, X., Zhang, J., Du, J., Xu, S., Tang, J., Zhang, Y., 2020. DFT studies on the reaction mechanism and kinetics of
554 dibutyl phthalate initiated by hydroxyl and sulfate radicals: Prediction of the most reactive sites. Chem. Eng. J. 381,
555 122680.

556 Lin, C., Zhang, L., Zhang, H., Wang, Q., Zhu, J., Wang, J., Qian, M., 2018. Enantioselective degradation of Myclobutanil
557 and Famoxadone in grape. Environ. Sci. Pollut. Res. 25, 2718–2725.

558 López, P., Méndez, F., 2004. Fukui function as a descriptor of the imidazolium protonated cation resonance hybrid structure.
559 Org. Lett. 6, 1781–1783.

560 Lu, T., Chen, F., 2012. Multiwfn: A multifunctional wavefunction analyzer. J. Comput. Chem. 33, 580–592.

561 Luo, S., Gao, L., Wei, Z., Spinney, R., Dionysiou, D.D., Hu, W.P., Chai, L., Xiao, R., 2018. Kinetic and mechanistic aspects
562 of hydroxyl radical–mediated degradation of naproxen and reaction intermediates. Water Res. 137, 233–241.

563 Machado, H.G., Sanches-Neto, F.O., Coutinho, N.D., Mundim, K.C., Palazzetti, F., Carvalho-Silva, V.H., 2019.
564 "Transitivity": A Code for Computing Kinetic and Related Parameters in Chemical Transformations and Transport
565 Phenomena. Molecules 24, 3478.

566 Manonmani, G., Sandhiya, L., Senthilkumar, K., 2020. Mechanism and kinetics of diuron oxidation by hydroxyl radical

addition reaction. Environ. Sci. Pollut. Res.

Manonmani, G., Sandhiya, L., Senthilkumar, K., 2019. Mechanism and Kinetics of Diuron Oxidation Initiated by Hydroxyl Radical: Hydrogen and Chlorine Atom Abstraction Reactions. J. Phys. Chem. A 123, 8954–8967.

Matta, C.F., Boyd, R.J., 2007. The Quantum Theory of Atoms in Molecules: From Solid State to DNA and Drug Design. John Wiley & Sons.

Mei, Q., Sun, J., Han, D., Wei, B., An, Z., Wang, X., Xie, J., Zhan, J., He, M., 2019. Sulfate and hydroxyl radicals-initiated degradation reaction on phenolic contaminants in the aqueous phase: Mechanisms, kinetics and toxicity assessment. Chem. Eng. J. 373, 668–676.

Melin, J., Ayers, P.W., Ortiz, J.V., 2007. Removing electrons can increase the electron density: a computational study of negative Fukui functions. J. Phys. Chem. A 111, 10017–10019.

Milenković, D.A., Dimić, D.S., Avdović, E.H., Amić, A.D., Dimitrić Marković, J.M., Marković, Z.S., 2020. Advanced oxidation process of coumarins by hydroxyl radical: Towards the new mechanism leading to less toxic products. Chem. Eng. J. 395, 124971.

Organization, W.H., others, 2006. Pesticides and their application: for the control of vectors and pests of public health importance.

Organization, W.H., others, 1990. Public health impact of pesticides used in agriculture. World Health Organization.

Özcan, A., Şahin, Y., Koparal, A.S., Oturan, M.A., 2008. Degradation of picloram by the electro-Fenton process. J. Hazard. Mater. 153, 718–727.

Planas, C., Caixach, J., Santos, F.J., Rivera, J., 1997. Occurrence of pesticides in Spanish surface waters. Analysis by high resolution gas chromatography coupled to mass spectrometry. Chemosphere 34, 2393–2406.

Rahman, M.A., Muneer, M., 2005. Heterogeneous photocatalytic degradation of picloram, dicamba, and floumeturon in aqueous suspensions of titanium dioxide. J. Environ. Sci. Heal. - Part B Pestic. Food Contam. Agric. Wastes 40, 247–

267.

Reuschenbach, P., Silvani, M., Dammann, M., Warnecke, D., Knacker, T., 2008. ECOSAR model performance with a large test set of industrial chemicals. Chemosphere 71, 1986–1995.

Rozas, I., Alkorta, I., Elguero, J., 2000. Behavior of ylides containing N, O, and C atoms as hydrogen bond acceptors. J. Am. Chem. Soc. 122, 11154–11161.

Sanches-Neto, F.O., Coutinho, N.D., Carvalho-Silva, V.H., 2017. A novel assessment of the role of the methyl radical and water formation channel in the CH 3 OH+ H reaction. Phys. Chem. Chem. Phys. 19, 24467–24477.

Sanches-Neto, F.O., Coutinho, N.D., Palazzetti, F., Carvalho-Silva, V.H., 2020. Temperature dependence of rate constants for the H(D) + CH_4 reaction in gas and aqueous phase: deformed Transition-State Theory study including quantum tunneling and diffusion effects. Struct. Chem. 31.

Sanches-Neto, Flávio O., Coutinho, N.D., Palazzetti, F., Carvalho-Silva, V.H., 2020. Temperature dependence of rate constants for the H(D) + CH4 reaction in gas and aqueous phase: deformed Transition-State Theory study including quantum tunneling and diffusion effects. Struct. Chem. 31, 609–617.

Sanches-Neto, F.O., S, J.R.D., Junior, L.H.K.Q., Carvalho-Silva, V.H., n.d. "pySiRC": Machine learning combined with molecular fingerprints to predict the reaction rate constant of the radical-based oxidation processes of aqueous organic contaminants. submitted.

Sanderson, H., Johnson, D.J., Wilson, C.J., Brain, R.A., Solomon, K.R., 2003. Probabilistic hazard assessment of environmentally occurring pharmaceuticals toxicity to fish, daphnids and algae by ECOSAR screening. Toxicol. Lett. 144, 383–395.

Seufert, V., Ramankutty, N., Foley, J.A., 2012. Comparing the yields of organic and conventional agriculture. Nature 485, 229–232.

Shemer, H., Sharpless, C.M., Elovitz, M.S., Linden, K.G., 2006. Relative rate constants of contaminant candidate list

611 pesticides with hydroxyl radicals. Environ. Sci. Technol. 40, 4460–4466.

612 Silva, M.P., Mostafa, S., McKay, G., Rosario-Ortiz, F.L., Teixeira, A.C.S.C., 2015. Photochemical Fate of Amicarbazone in

613 Aqueous Media: Laboratory Measurement and Simulations. Environ. Eng. Sci. 32, 730–740.

614 Silva, V.H.C., Camargo, L., Napolitano, H.B., Pérez, C.N., Camargo, A.J., 2010. Theoretical investigation of the interaction

615 of glycerol with aluminum and magnesium phthalocyanines. J. Mol. Graph. Model. 29, 206–213.

616 Socorro, J., Durand, A., Temime-Roussel, B., Gligorovski, S., Wortham, H., Quivet, E., 2016. The persistence of pesticides

617 in atmospheric particulate phase: An emerging air quality issue. Sci. Rep. 6, 1–7.

618 Son, Y., Lee, Y.M., Zoh, K.D., 2020. Kinetics and degradation mechanism of tris (1-chloro-2-propyl) phosphate in the

619 UV/H2O2 reaction. Chemosphere 260, 127461.

620 Spadotto, C.A., Hornsby, A.G., 2003. Soil sorption of acidic pesticides: Modeling pH effects. J. Environ. Qual. 32, 949–

621 956.

622 Stapleton, D.R., Konstantinou, I.K., Mantzavinos, D., Hela, D., Papadaki, M., 2010. On the kinetics and mechanisms of

623 photolytic/TiO2-photocatalytic degradation of substituted pyridines in aqueous solutions. Appl. Catal. B Environ. 95,

624 100–109.

625 Tomlin, C.D.S., others, 2009. The pesticide manual: A world compendium. British Crop Production Council.

626 Tremolada, P., Finizio, A., Villa, S., Gaggi, C., Vighi, M., 2004. Quantitative inter-specific chemical activity relationships

627 of pesticides in the aquatic environment. Aquat. Toxicol. 67, 87–103.

628 Truong, T.N., Truhlar, D.G., Baldridge, K.K., Gordon, M.S., Steckler, R., 1989. Transition state structure, barrier height,

629 and vibrational frequencies for the reaction Cl+ CH4→ CH3+ HCl. J. Chem. Phys. 90, 7137–7142.

630 Vasileiadis, V.P., 2017. Economic sustainability: Less pesticide rarely causes loss. Nat. Plants 3.

631 Wauchope, R.D., Buttler, T.M., Hornsby, A.G., Augustijn-Beckers, P.W.M., Burt, J.P., 1992. The SCS/ARS/CES pesticide

632 properties database for environmental decision-making, in: Reviews of Environmental Contamination and

633 Toxicology. Springer, pp. 1–155.

634 Wenk, J., Gunten, U. Von, Canonica, S., 2011. Effect of dissolved organic matter on the transformation of contaminants

635 induced by excited triplet states and the hydroxyl radical. Environ. Sci. Technol. 45, 1334–1340.

636 Yan, B., Xu, D.C., Liu, Z., Tang, J., Huang, R., Zhang, M., Cui, F., Shi, W., Hu, C., 2021. Degradation of neurotoxin

637 β-N-methylamino-L-alanine by UV254 activated persulfate: Kinetic model and reaction pathways. Chem. Eng. J.

638 404, 127041.

639 Yanai, T., Tew, D.P., Handy, N.C., 2004. A new hybrid exchange-correlation functional using the Coulomb-attenuating

640 method (CAM-B3LYP). Chem. Phys. Lett. 393, 51–57.

641 Yang, J., Wang, Z., Lv, G., Liu, W., Wang, Y., Sun, X., Gao, J., 2020. Indirect photodegradation of fludioxonil by hydroxyl

642 radical and singlet oxygen in aquatic environment: Mechanism, photoproducts formation and eco-toxicity

643 assessment. Ecotoxicol. Environ. Saf. 197, 110644.

644 Yang, X., Cao, X., Zhang, L., Wu, Y., Zhou, L., Xiu, G., Ferronato, C., Chovelon, J.-M., 2020. Sulfate radical-based

645 oxidation of the aminopyralid and picloram herbicides: the role of amino group on pyridine ring. J. Hazard. Mater.

646 124181.

647 Yang, Z., Su, R., Luo, S., Spinney, R., Cai, M., Xiao, R., Wei, Z., 2017. Comparison of the reactivity of ibuprofen with

648 sulfate and hydroxyl radicals: An experimental and theoretical study. Sci. Total Environ. 590–591, 751–760.

649 Zhang, L., Truhlar, D.G., Sun, S., 2020. Association of Cl with C2H2 by unified variable-reaction-coordinate and

650 reaction-path variational transition-state theory. Proc. Natl. Acad. Sci. U. S. A. 117, 5610–5616.

651

652

FIGURE CAPTIONS

Figure 8: Scheme of hydrogen atom abstraction and addition reactions with picloram and •OH radicals.

Figure 9: Illustration of the setup used in the competition kinetics and photolysis experiments.

Figure 10: Pseudo-first-order plots of picloram and pCBA in the hydroxyl radical reaction system.

Figure 11: Fukui function values for the •OH radical attack on selected carbon atoms of picloram in water (see nomenclature in Figure 1).

Figure 12: Relative energy profile corresponding to the initial abstraction of the hydrogen atom and picloram addition reaction by the •OH radical.

Figure 13: Half-life time, in days, of picloram degradation as a function of •OH concentration, in mol L^{-1}, in the temperature range 273.15-310 K in natural waters.

Figure 14: UV-VIS absorption spectra of picloram and degradation by-products calculated at the (TD)CAM-B3LYP/6-311++G(d,p) level of theory. The experimental value is also presented for comparison (Dos Santos et al., 2010).